ELSEVIER

Tectonophysics 336 (2001) 121–136

TECTONOPHYSICS

www.elsevier.com/locate/tecto

Alpine metamorphism and veining in the Zentralgneis Complex of the SW Tauern Window: a model of fluid–rock interactions based on fluid inclusions

Bernardo Cesare[a,*], Elena Poletti[a,1], Marie-Christine Boiron[b,2], Michel Cathelineau[b,2]

[a] *CNR, Centro di Studio per la Geodinamica Alpina and Dipartimento di Mineralogia e Petrologia, Università di Padova, Corso Garibaldi, 37 I-35137 Padova, Italy*
[b] *G2R and CREGU BP 23 54501 Vandoeuvre-les-Nancy, France*

Abstract

The granitic to tonalitic gneisses of the Zentralgneis Complex in the SW Tauern Window contain numerous discordant quartz–biotite–plagioclase veins occurring either as isolated or in parallel sets with a preferential orientation perpendicular to the main foliation of host rocks. Veins show a zonal distribution of minerals with plagioclase and biotite at the walls and quartz in the centre. Quartz contains abundant fluid inclusions (FI) mostly occurring along secondary planes; all 'primary' and most secondary inclusions (three-phase H_2O–CO_2 inclusions) formed from a dominant fluid type of aqueous-carbonic composition.

FI have been characterized by microthermometry, laser Raman and laser ablation-optical emission spectroscopies, which have confirmed their similarity also with respect to composition and density. Fluids display a somewhat unusual composition, especially a wide range of rather high salinities (3–7 mol%) deduced from the final melting temperature of clathrate, which covers a wide range from −4.2 to +4.0°C. The volatile phase is dominated by CO_2 (3–12 mol%) with small amounts of N_2. The final homogenization temperature of these inclusions is generally >300°C, but independently constrained trapping temperatures of 550–600°C yield to pressure estimates of 3.5–7.5 kbar. Highest pressures are in agreement with the P–T conditions reached during the Tauern metamorphism peak. Veining was triggered by hydrofracturing induced by Pl–Bt-producing devolatilization and probably decarbonation reactions in the adjacent gneisses, and quartz precipitated in response to the significant pressure and/or salinity fluctuations shown by FI during each microfracturing/healing stage.

Keywords: fluid inclusions; synmetamorphic veins; Tauern Window; Zentralgneis Complex

1. Introduction

Metamorphic veins and segregations, especially those with pegmatitic structure, are generally interpreted as the product of crystallization from a fluid (aqueous) and represent one of the most evident examples of fluid–rock interaction during metamorphism. Numerous problems are related to the interpretation of the genesis of metamorphic veins: they involve the cause and mechanisms of fracturing, the type of fluid that occurred in the fracture and its origin, the mechanism(s) of mass-transfer, and the amount of fluid that passed through the fracture.

The type of fluid can be successfully constrained by

* Corresponding author. Fax: +39-0498272010.
E-mail addresses: bernardo@dmp.unipd.it (B. Cesare), michel.cathelineau@g2r.uhp-nancy.fr (M. Cathelineau).
[1] Fax: +39-0498272010.
[2] Fax: +33-3-83-91-38-01.

0040-1951/01/$ - see front matter
PII: S0040-1951(01)00097-X

the analysis of primary and secondary fluid inclusions (FI) in vein minerals, which also helps defining the possible P–T conditions of vein formation. As far as the problem of the source of fluids in the veins is concerned, it has been approached by several methods, among which FI and stable isotopic studies play a major role. The mechanisms of fluid flow during regional metamorphism have been addressed in the review of Oliver (1996), who classified the two end-member types of flow as closed system (i.e. internally controlled) and open system (i.e. externally controlled), and related them to specific tectonic scenarios characterized in terms of strain and permeability.

In an open system, the fluids which pervade already opened fractures may be in chemical and/or mechanical and/or thermal disequilibrium with the host rock: the resulting non-equilibrium interaction is generally called 'infiltration metasomatism' (Kerrick, 1990) and often produces veins with extensive metasomatic features such as diffusion halos in the wall rock. In an open system, the mineralogy of vein minerals may be completely unrelated to that of the host rocks.

In the closed system behaviour, as fluid is generally released during devolatilization reactions, veining should reflect (and be controlled by) the type of reaction occurring in the host rocks. Thus, veins forming in a closed system may be recognizable from peculiar mineralogical features, and reactions bringing to their development may be deduced (e.g. Cesare, 1994). Processes at the origin of mineral precipitation are important also to consider, especially those linked to fluid pressure fluctuation that can strongly affect dissolution and precipitation of minerals, especially quartz which constitutes the main vein infilling in such a context.

This work describes the results of the FI study performed on some quartz–biotite–plagioclase veins occurring in the Zentralgneis Complex of the Tauern Window, an area where numerous veining events occurred along the Alpine polymetamorphic sequence and where the Alpine P–T–t history is quite well constrained. The aims of this study are as follows: (i) a test on some natural examples, to argue for or against one of the above models of fluid flow, and (ii) combining structural and petrological data in addition to a detailed FI study to determine the P–T conditions of vein formation.

2. Geologic framework

The Tauern Window is the largest tectonic window in the Eastern Alps and is the only one that exposes a complete cross-section through the Penninic sequence beneath the overthrust Austro-Alpine nappes (Frisch et al., 1993 and references therein). Within the Tauern Window, the Zentralgneis Complex is a granitoid batholith of Carboniferous age, mainly between 330 and 300 Ma (Finger et al., 1993; Frisch et al., 1993). The Zentralgneis complex represents the lowest Penninic structural unit overlain by the Lower and Upper Schieferhülle (Morteani, 1974) and is formed by several intrusions which display variable chemical composition (D'Amico, 1974) ranging from granite to diorite with rare ultramafic cumulates (Barzi and Cesare, 1996). Most granitoids in the Zentralgneis are biotite-bearing granodiorites or granites with a typical I-type geochemical signature.

As the neighbouring units of the Tauern Window, the Zentralgneis Complex was deeply affected by Alpine deformation and metamorphism (Morteani, 1974; Raith, 1971; Raith et al., 1978) involving an early stage characterized by blueschist to eclogite-facies conditions (Selverstone, 1985) followed by decompression to 5–7 kbar and thermal peak at 650°C during the Oligocene 'Tauern metamorphism' (Hoernes and Friedrichsen, 1974; Friedrichsen and Morteani, 1979). This P–T evolution reflects the complex tectonic history of the Alpine margin, involving subduction, continent–continent collision and final extension (Selverstone, 1988 and references therein). The Tauern metamorphism corresponds to the 'Tauernkrystallisation' of Sander (1921) and to the M_a2 event of Holland (1979).

The area studied is located in the Neves region at the south-western margin of the Zentralgneis complex (Fig. 1) and represents the periphery of a granitoid dome (the Zillertal massif, Morteani, 1974) about 2 km to the north of the tectonic contact with the Paleozoic and Mesozoic sequences of the Lower and Upper Schieferhülle (De Vecchi and Baggio, 1982; De Vecchi and Mezzacasa, 1986). In this area, the othogneisses of the Zentralgneis complex are mainly represented by metagranites and metatonalites with minor quartz–diorites and rare gabbros. The structure of these rocks ranges from strongly foliated to undeformed proceeding to the north, i.e. away from

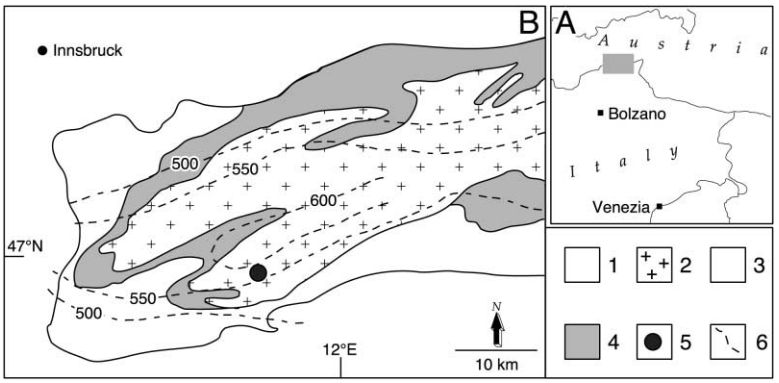

Fig. 1. (A) Location (shaded box) and (B) schematic geologic map of the western Tauern Window modified after Selverstone (1985): (1) Austro-alpine basement; (2) Zentralgneis Complex; (3) Upper Schieferhülle; (4) Lower Schieferhülle; (5) location of study area in the upper Neves valley; (6) isotherms of the maximum temperature during the Tauern metamorphism (from Hoernes and Friedrichsen, 1974).

the tectonic boundary where Alpine deformation was more intense (De Vecchi and Mezzacasa, 1986). As noted by Morteani (1974), even the isotropic rocks that have maintained a magmatic texture have undergone a complete metamorphic recrystallization during the thermal maximum of the Oligocene Tauern metamorphism. The maximum temperatures attained during the Tauern metamorphism are shown by the isotherms in Fig. 1, which run approximately E–W subparallel to the southern border of the Tauern Window, and indicate values in the range 550–600°C for the orthogneisses of the Neves area. According to Christensen et al. (1994), the thermal maximum in the western Tauern Window was attained at ca. 30 Ma.

The veins in the Zentralgneis have been investigated by several methods: the systematics of oxygen and hydrogen isotopes (Hörmann and Morteani, 1972; Hoernes and Friedrichsen, 1974; Friedrichsen and Morteani, 1979) indicate that minerals of veins and host rocks have formed or recrystallized at similar temperatures during the thermal peak of the Tauern metamorphism (i.e. between 500 and 600°C). Based on chemical, microthermometric and neutron activation data on FI from numerous vein samples, Luckscheiter and Morteani (1980) concluded that quartz veins typically contain fluids with low CO_2/H_2O ratios and high salinity (NaCl dominated), and that the veins formed in an extensional regime related to the updoming of the central part of the Tauern Window. Luckscheiter and Morteani (1980) argued that the composition of the FI should correspond to that of fluids in the host rocks, except for the CO_2 component, that was considered of external derivation because of the scarcity of carbonates in the area.

3. The quartz veins and their host rocks

3.1. Host rocks

The metagranites and granitic gneisses hosting the veins have been previously described by Morteani and Raase (1974). In the host rocks, the foliation is absent or very weak except for rare occurrences, where cm- to dm-thick shear zones are observed. The mineral assemblage of host gneisses is Qtz, Pl, Bt, Ms, Ep ± Grt ± Chl ± Cal ± Kfs (mineral abbreviations by Kretz, 1983). Even in the foliated rocks, the microstructure is granofelsic with random orientation of all mineral phases in the different compositional layers.

Quartz from the primary granitoid is almost completely recrystallized to fine-grained aggregates of undeformed crystals, and is only in some places preserved as coarse relicts characterized by deformation bands. Plagioclase occurs as anhedral inversely zoned poikilitic crystals, rich in inclusions of muscovite, epidote and quartz. These inclusions may be concentrated at the core of plagioclase. Muscovite occurs in preferential sites at the boundary of plagioclase-rich layers, where it forms aggregates of fine-grained lamellae with random orientation. Biotite

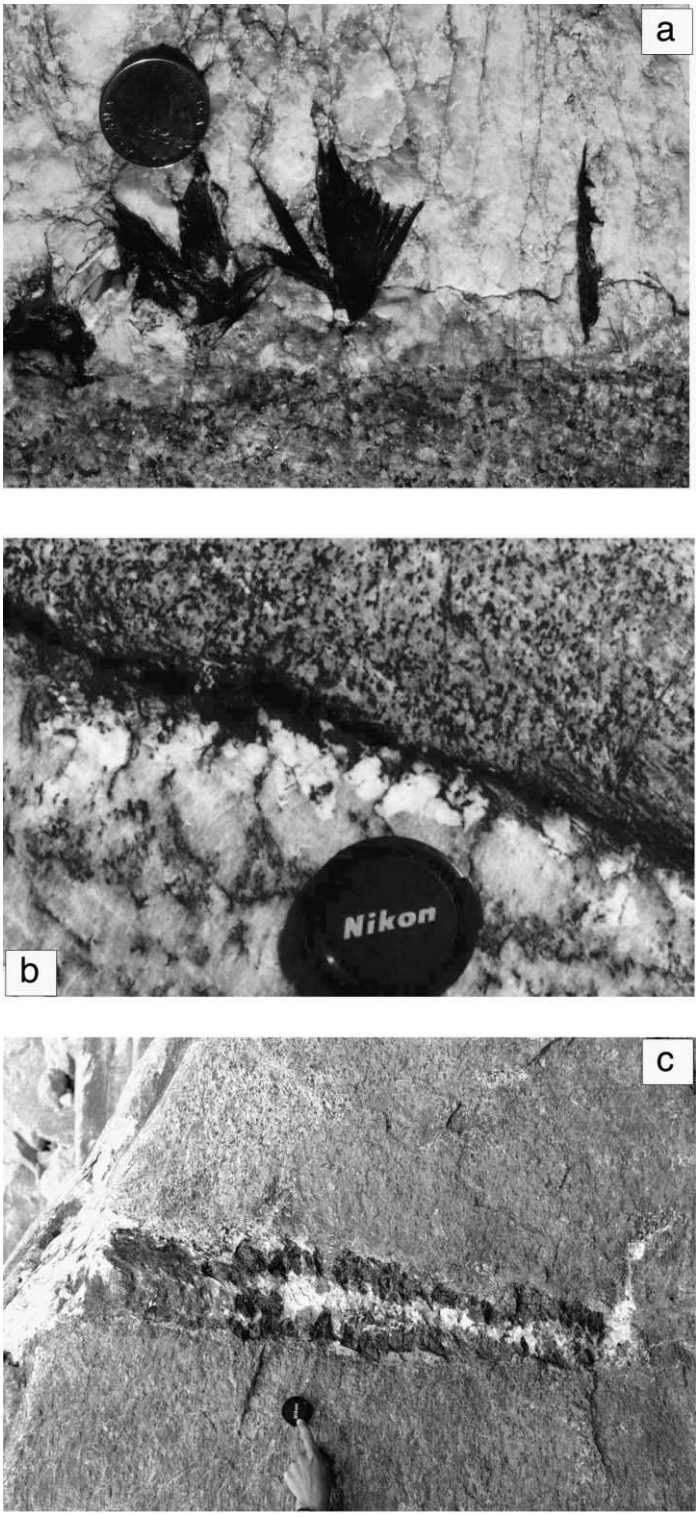
a
Nikon
b
c

is euhedral and fine-grained and forms polycrystalline aggregates or layers, often with decussate structure. A common feature of biotite is the abundance of epidote inclusions: the resorbed shape, geometric arrangement and coherent optical orientation of these inclusions suggest that they represent relicts from a former metamorphic assemblage altered into biotite. This is supported by the presence of epidote inclusions also in plagioclase. Garnet occurs as rare fine-grained (<0.5 mm) euhedral crystals.

Many granite gneisses of the Neves area also contain K-feldspar and/or calcite; calcite appears in textural equilibrium with the mineral assemblage described above and does not represent a late-stage product of alteration or fluid infiltration, such as chlorite.

The microstructural evidence confirms the conclusions of earlier works (e.g. Morteani and Raase, 1974) that the main deformation of the orthogneisses, including development of foliation and local mylonitic fabric, predates extensive recrystallization that occurred at static conditions.

3.2. The veins: field and microscopic observations

About 170 veins have been studied in the Neves area. Most veins consist of quartz but both Qtz–Cal and Qtz–Pl–Bt veins are present; the latter type is the subject of this fluid inclusion study and unless specified, all the data and observations that follow refer to this. Veins display minerals of coarser grain size (1–2 cm, exceptionally 5 cm) with respect to the host gneiss, where the average grain size is <5 mm. Veins show a zonal distribution of minerals (Fig. 2a) with euhedral cm-sized plagioclase and biotite concentrated at vein walls and often elongate perpendicular to them (Fig. 2b). Quartz is the most abundant (up to 90 vol%) mineral in the veins, but there are examples where biotite is very abundant (Fig. 2c). Locally, plagioclase and biotite crystals occur within the vein, forming alignments parallel to the wall rocks; this mineral distribution is probably indicative of repeated fracturing events during veining, as in the crack-seal mechanism (Ramsay, 1980).

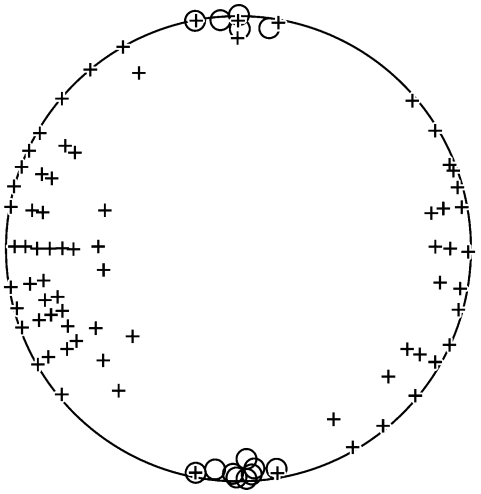

Fig. 3. Stereographic projection of poles of Qtz–Pl–Bt veins (crosses) and foliations in host gneisses (circles).

The veins occur as both planar or irregular in shape with maximum length of 5 m and maximum thickness of about 1 m. They are either isolated or in parallel sets and maintain quite a constant orientation, with maximum distribution around N–S subvertical, over an area of several km^2. The host rocks are mainly undeformed to weakly foliated granodioritic and granitic gneisses. In some places, these rocks show an E–W foliation perpendicular to the N–S orientation of the veins (Fig. 3). The Qtz–Pl–Bt veins have the same N–S subvertical orientation as veins consisting only of quartz.

In most occurrences, the host gneisses do not show evidence of metasomatic halos around veins, except for rare cm-thick dark border zones where a relative enrichment of mafic minerals can be observed. Although most veins were not deformed after their formation, in places they were involved in late-stage ductile and brittle deformation accompanied by widespread chloritization of biotite.

Under the microscope, considering the least strained and weathered vein samples, quartz is generally weakly deformed with minor undulose extinction and deformation lamellae. Conversely, in the most

Fig. 2. (a,b) Examples of the macroscopic appearance of Qtz–Pl–Bt veins in massive granodioritic gneisses. In both cases, plagioclase and biotite are located at vein borders and quartz in the inner part. (c) Tapered termination of a Qtz–Pl–Bt vein. Note the abundance of biotite at vein walls.

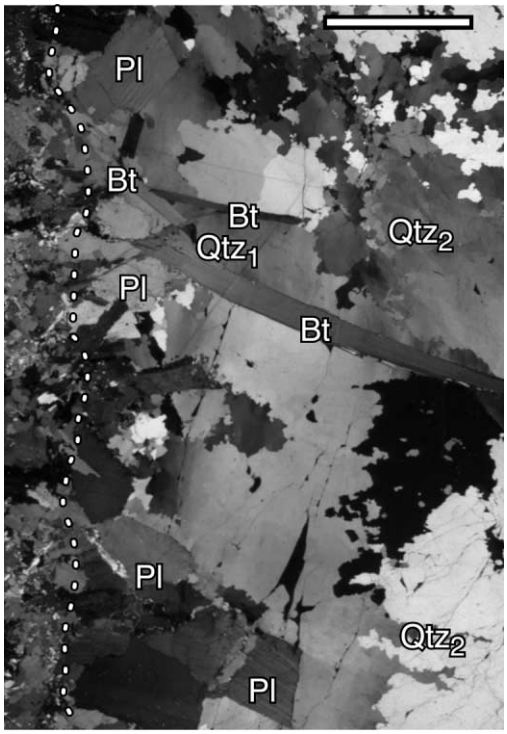

Fig. 4. Photomicrograph showing the typical microscopic appearance of Qtz–Pl–Bt veins. Biotite (Bt) and plagioclase (Pl) grow as euhedral crystals projecting into the vein from the contact. Quartz fills most of the vein with variable degrees of strain: undeformed or slightly deformed crystals (Qtz_1) occur adjacent to plagioclase or biotite, whereas in the vein centre quartz is much more deformed (Qtz_2) and shows extensive recrystallization. Dotted line marks the vein–host contact: note the difference of grain size between vein and host rock. Crossed polars; scale bar ca. 1 cm.

deformed samples, the milky quartz shows formation of subgrain boundaries; in this case, undeformed crystals are rare and mostly occur close to vein walls embedded in or protected by the plagioclase–biotite, border zone (Fig. 4). Plagioclase is euhedral, has a weak concentric zoning and is rarely twinned. Biotite lamellae extend from the vein wall toward the vein core (Fig. 4) and sometimes form radiating aggregates as in Fig. 2a.

3.3. Mineral compositions

The composition of minerals was analysed in two vein samples and their host gneisses with the CAMECA Camebax electron microprobe of CNR at the Department of Mineralogy and Petrology, University of Padova. Working conditions were 15 kV accelerating voltage and 15 nA sample current; natural and synthetic silicates and oxides were used as standards and the beam diameter was generally focussed to ca. 1 μm. Representative analyses are reported in Table 1.

The compositions of biotite is similar in the two veins ($X_{Fe} = 0.60$–0.64, Ti ≈ 0.3 atoms) and is identical to biotite in the respective hosts. This also applies to the chlorine content that ranges from 0.10 to 0.18 wt%. Assuming stoichiometry, the H_2O/Cl ratio of biotites is 0.01–0.02. In the gneiss, plagioclase shows a weak inverse zoning from An_{15} at the core to An_{25} in the rim, in agreement with the observations of Morteani and Raase (1974). In the veins, plagioclase compositions vary in the same interval, but are generally $\geq An_{20}$.

Epidote and muscovite have similar compositions in both gneiss samples regardless of their textural position. Muscovite has low paragonite content and low (<25%) celadonite substitution. Garnet (present in only one sample) is an almandine-grossular solid solution within the compositional range $Alm_{63-66}Grs_{26-30}Pyp_{3-6}Sps_{1-6}$. Similar Ca-rich compositions in a biotite–oligoclase–epidote assemblage are interpreted by Le Goff (1989) as typical of granitic orthogneisses metamorphosed under amphibolite-facies conditions.

4. The fluid inclusions

Most FI in vein quartz display similar features and occur either (i) as rare isolated inclusions (Fig. 5) or small clusters without preferred spatial arrangement. The origin of these FI that are located in undeformed or weakly deformed quartz is probably 'primary'; (ii) more commonly as secondary FI in arrays of parallel planes that generally cut across the grain boundaries of quartz (Figs. 6 and 7). FI display generally an irregular shape (Fig. 7) and range in size from 20 to 60 μm (Fig. 8) with the exception of some possibly primary FI with negative crystal shape that are smaller (<30 μm in size, see Fig. 5). Both primary and secondary FI are aqueous-carbonic solutions (noted Lc-w) with similar degree of volatile filling (20–40 vol%, visually estimated) except for very rare

Table 1
Representative electron microprobe analyses of minerals in host gneiss and vein from two samples (V2A and V2C)

Phase sample	Ep V2A gneiss	Ep V2C gneiss	Phase sample	Pl (rim) V2A gneiss	Pl (core) V2A gneiss	Pl V2A vein	Pl V2A vein	Pl (rim) V2C gneiss	Pl (core) V2C gneiss	Pl (rim) V2C vein	Pl (core) V2C vein
SiO_2	38.69	38.38	SiO_2	64.48	64.69	64.67	65.13	64.06	62.46	62.64	62.68
TiO_2	0.23	0.08	Al_2O_3	22.86	22.65	22.66	22.38	22.10	23.18	23.51	23.23
Al_2O_3	28.05	27.54	FeO	0.00	0.00	0.01	0.07	0.00	0.03	0.02	0.06
Fe_2O_3	6.53	7.16	MgO	0.00	0.00	0.00	0.00	0.00	0.00	0.02	0.02
MnO	0.07	0.21	CaO	3.85	3.35	3.86	3.48	3.58	4.95	5.53	5.05
CaO	23.39	23.54	Na_2O	9.38	9.73	9.30	9.47	9.32	8.63	9.00	8.71
Na_2O	0.00	0.00	K_2O	0.22	0.19	0.26	0.27	0.30	0.25	0.23	0.22
Total	96.96	96.91	Total	100.79	100.61	100.76	100.80	99.36	99.49	100.95	99.97
Si	3.03	3.02	Si	2.82	2.83	2.83	2.85	2.84	2.78	2.76	2.78
Ti	0.01	0.00	Al	1.18	1.17	1.17	1.15	1.16	1.22	1.22	1.21
Al	2.59	2.55	Fe	0.00	0.00	0.00	0.00	0.00	0.00	0.00	0.00
Fe^{3+}	0.38	0.42	Mg	0.00	0.00	0.00	0.00	0.00	0.00	0.00	0.00
Mn	0.01	0.01	Ca	0.18	0.16	0.18	0.16	0.17	0.24	0.26	0.24
Ca	1.96	1.98	Na	0.80	0.83	0.79	0.80	0.80	0.74	0.77	0.75
Na	0.00	0.00	K	0.01	0.01	0.02	0.02	0.02	0.01	0.01	0.01
			% An	0.19	0.16	0.19	0.17	0.18	0.24	0.25	0.24
Oxygens	12	12	Oxygens	8	8	8	8	8	8	8	8

Phase sample	Grt (rim) V2C gneiss	Grt (core) V2C gneiss	Phase sample	Bt V2A vein	Bt V2A gneiss	Bt V2C vein	Bt V2C gneiss	Ms V2A gneiss	Ms V2C gneiss
SiO_2	37.65	37.16	SiO_2	35.99	36.24	35.31	36.13	47.79	47.00
TiO_2	0.08	0.01	TlO_2	2.45	2.75	2.64	2.70	0.76	0.62
Al_2O_3	20.89	20.75	Al_2O_3	7.17	17.00	16.64	16.48	32.53	30.54
FeO	30.08	28.37	FeO	22.45	22.81	22.98	22.95	3.04	3.47
MnO	0.57	2.59	MnO	0.15	0.23	0.11	0.21	0.00	0.00
MgO	1.17	0.76	MgO	7.90	7.74	7.46	7.31	1.30	1.91
CaO	10.32	9.97	CaO	0.00	0.00	0.00	0.01	0.02	0.00
Total	100.77	99.65	Na_2O	0.07	0.07	0.07	0.03	0.23	0.26
			K_2O	8.92	8.98	9.31	9.40	9.97	10.40
Si	5.99	5.99	Cl	0.15	0.13	0.18	0.15	0.01	0.00
Al^{IV}	0.01	0.01	Total	95.25	95.95	94.70	95.37	95.65	94.20
Al^{VI}	3.91	3.94							
Ti	0.01	0.00	Si	5.56	5.56	5.53	5.61	6.36	6.40
Fe^{2+}	4.00	3.83	Al^{IV}	2.44	2.44	2.47	2.39	1.64	1.60
Mn	0.08	0.35	Al^{VI}	0.68	0.64	0.60	0.62	3.46	3.30
Mg	0.28	0.18	Ti	0.28	0.32	0.31	0.32	0.08	0.06
Ca	1.76	1.72	Fe^{2+}	2.90	2.93	3.01	2.98	0.34	0.40
X_{Fe}	0.94	0.95	Mn	0.02	0.03	0.02	0.03	0.00	0.00
			Mg	1.82	1.77	1.74	1.69	0.26	0.39
% Alm	0.65	0.63	Ca	0.00	0.00	0.00	0.00	0.00	0.00
% Grs	0.29	0.28	Na	0.02	0.02	0.02	0.01	0.06	0.07
% Pyp	0.05	0.03	K	1.76	1.76	1.86	1.86	1.69	1.81
% Sps	0.01	0.06	Cl	0.03	0.03	0.04	0.03	0.00	0.00
Oxygens	12	12	X_{Fe}	0.61	0.62	0.63	0.64	0.57	0.50
			Oxygens	22	22	22	22	22	22

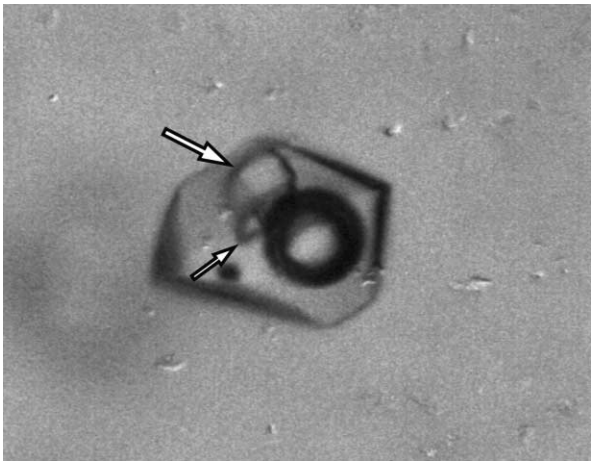

Fig. 5. Isolated (negative crystal) Lc-w FI of primary origin in quartz. The arrows indicate two daughter crystals. Inclusion length is approximately 20 μm.

aqueous FI (noted Lw) in fluid inclusion planes (FIP). Lc-w inclusions contain three fluid phases at room temperature. Additional solids are frequent (one or two) and birefringent crystals (Figs. 5 and 8), generally small in size (<5 μm). Raman spectra of the solids suggest that one of them is calcite (band at 1082 cm^{-1}). As primary and secondary inclusions show a similar behaviour also from a microthermometric point of view, they are described together.

Representative vein samples were selected for the microthermometric analysis, performed on doubly polished 100 μm-thick wafers on a total of about

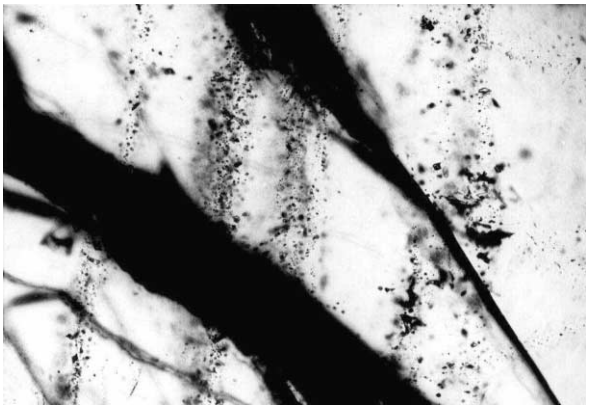

Fig. 6. Parallel planes of Lc-w FI in quartz. Note that the planes cut across grain boundaries (larger black band). Width of view ca. 3 mm.

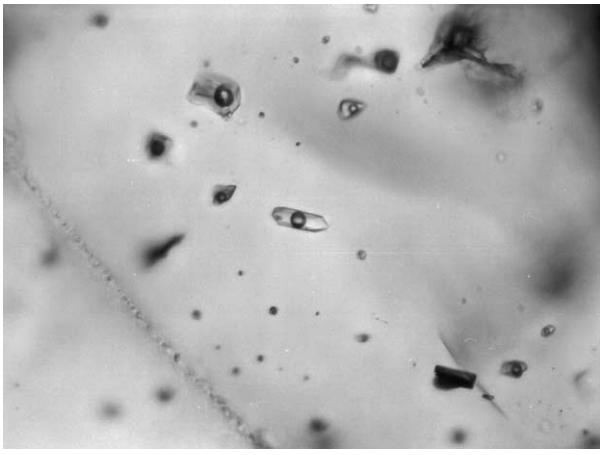

Fig. 7. Plane of secondary Lc-w FI in quartz. FI exhibit both irregular and negative crystal shape. Width of view ca. 0.2 mm.

100 FI representative of the various populations. Temperature measurements were obtained using a LINKAM TH600 heating–freezing stage and could be reproduced within errors and accuracy of ±0.1°C in the interval −100/+100°C and ±1°C at $T > 200$°C. Phase transitions at $T < 32$°C were observed at a heating rate of 0.5°C/min. Results are summarized in Fig. 9, and Tables 2 and 3.

In volatile-bearing FI, CO_2 was identified by the melting of a solid below −56.6°C. The volumetric fraction of the aqueous liquid (flw) and the volumetric fraction of the volatile-rich liquid (CO_2 dominated liquid) in the volatile-rich phase (flc) have been

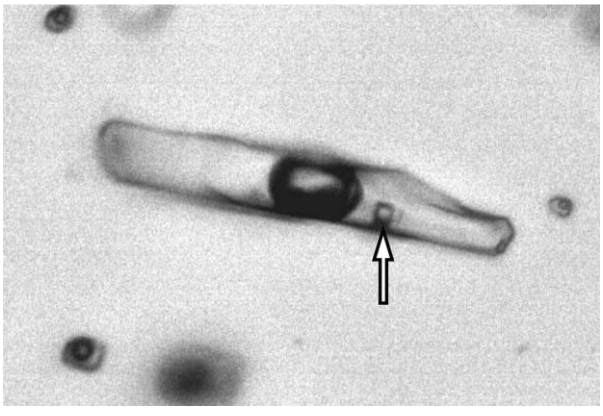

Fig. 8. Large irregular Lc-w FI of secondary origin. Arrow: daughter crystal. Inclusion length is approximately 50 μm.

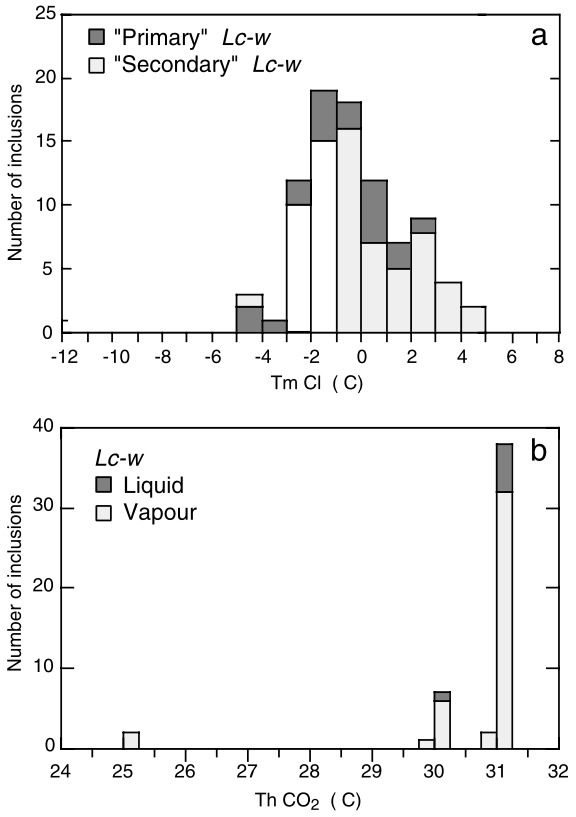

Fig. 9. (a) Histogram of the final melting temperature of clathrate (T_m Cl). (b) Histogram of the homogeneization temperature of CO_2 (T_h CO_2) of Lc-w FI.

estimated at room temperature using the volumetric chart of Roedder (1984). After preliminary studies by C. Maineri (CNR Firenze) molar fractions of CO_2, N_2 and Cl were determined in individual FI by micro-Raman analysis performed on a DILOR LABRAM Raman spectrometer at CREGU, Nancy.

The volatile fraction of Lc-w FI is composed mostly of CO_2, with minor content of N_2 (0.5–2.2 mol%), as indicated by values of T_m CO_2 near −56.6 and confirmed by laser Raman spectroscopy (Table 2). Eutectic temperature is around −24°C, suggesting that NaCl is the dominant salt, other dissolved salts being only present in minor amounts. This is confirmed by laser ablation-optical emission spectroscopy (LA-OES) data, which show that Na is by far the dominant cation in solution, as emission lines for K, Ca, Mg and Li are below the detection level.

In all Lc-w FI, only one final melting event could be observed at temperatures ranging from −4.4 to +4°C, which corresponds to melting of the clathrate (T_m Cl), as confirmed by (i) Raman spectroscopy, (ii) V–X calculations, especially the agreement between calculated Cl content using T_m Cl and measured chlorine content by Raman spectroscopy (see below). From the distribution of T_m Cl in Fig. 9a, it is apparent that primary and secondary FI display similar features. The final melting temperatures cluster around a maximum at about −1°C with a continuous change from positive to negative T_m Cl values, corresponding a rather wide range of chlorinity.

Homogenization of CO_2 (T_h CO_2) occurs for most inclusions either to the liquid or to the vapour phase in between +30 and +31°C. Owing to their high bulk density, most FI decrepitated before homogenization at temperatures up to 350°C; the few measured final homogenization events (T_h) occurred in the range 280–335°C to the liquid phase. Up to 550°C and leaving the FI at high temperatures for a few hours, the

Table 2
Typology of FI in the analysed Qtz–Pl–Bt veins (Td: decrepitation temperature; nm: not measured. All temperatures are given in °C.)

Inclusion type	Main components	Habitus	Solids	T_m CO_2	T_h CO_2	T_m Cl	T_m H_2O	T_h
Lc-w	H_2O–CO_2–(N_2)–NaCl	Primary	0–2	−56.6 ($n = 24$)	30/31 (L or V)	−4.2/2.0 ($n = 24$)		325/330 or T_d = 300/340
Lc-w	H_2O–CO_2–(N_2)–NaCl	Secondary	0–2	−56.6 ($n = 52$)	25/31 (L or V) ($n = 44$)	−2.5/4.0 ($n = 52$)		280/310 or T_d = 250/330
Lwl	H_2O–NaCl	Secondary	0				−13.5/−13.8 ($n = 2$)	260
Lw2	H_2O–NaCl	Secondary	0–2				−0.3/−0.5 ($n = 8$)	nm

Table 3
Microthermometric results Raman data and calculated bulk compositions of selected FI (nd: not detected. All temperatures are given in °C)

Sample	Inclusion	Microthermometry (°C)			Raman (mol%)			Bulk composition (mol%)				
		T_h CO_2	Mode	T_m Cl	CO_2	CH_4	N_2	H_2O	CO_2	CH_4	N_2	NaCl
V2AI-B	1	31	L	−2.0	98.2	nd	1.8	80.8	13.4	–	0.2	5.6
V2AI-B	2	31	V	−2.2	99.1	nd	0.9	84.0	10.1	–	0.1	5.8
V2AI-B	3	30	V	−1.5	99.4	nd	0.6	86.9	7.3	–	< 0.05	5.8
V2AI-B	4	30	L	2.0	97.8	nd	2.2	87.1	8.4	–	0.2	4.3
V2AI-D	1	30	V	−2.4	98.4	nd	1.6	87.9	5.8	–	< 0.1	6.3
P-D	1	31	V	3.6	99.5	nd	0.5	87.0	9.4	–	< 0.05	3.5

daughter crystals did not show any sign of dissolution indicating that they could be considered as (i) mechanically trapped solids or (ii) daughter minerals displaying slow dissolution kinetics.

Based on the microthermometric data, studied FI can be modelled in the H_2O–CO_2–N_2–NaCl system using the code of Bakker (1997). The salinity is expressed either in mol% 'equivalent' NaCl or in wt% equivalent NaCl in the H_2O–CO_2–NaCl system, as NaCl is the dominant salt Na^+ and Cl^- being the dominant ion identified by Raman and LA-OES spectroscopies. It can be noted that conversion from mol% (bulk composition) to eq. wt% NaCl needs to consider the relative abundance of volatile species. Chlorinity has been estimated from Raman spectrum of water using methods of Dubessy et al. (1997) and Lhomme et al. (1999). The method is based on the calibration of difference in Raman spectra of pure water and known solution with respect to Cl^- concentration for known systems, especially the H_2O–NaCl–$CaCl_2$ system.

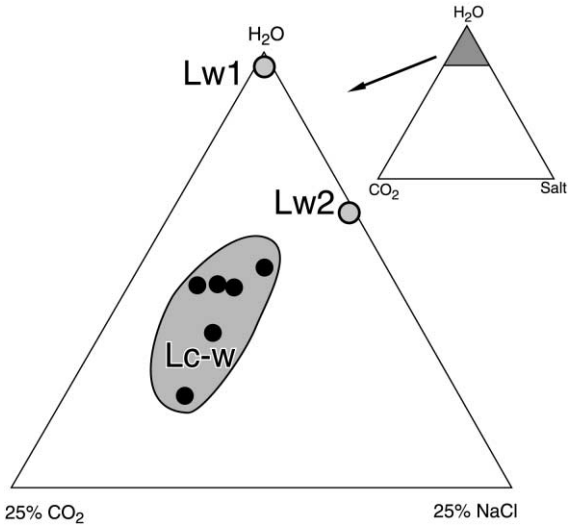

Fig. 10. Composition of Lc-w and Lw FI inclusion types in the system H_2O–CO_2–$NaCl_{eq}$.

Most representative inclusions are filled by a H_2O–CO_2–(N_2) mixture (80–88 mol% H_2O), with CO_2 contents in the range 5–13 mol%, and N_2 in the range 0.05–0.2 mol%. Extreme calculated and measured salinities are from 3 to 7 mol% NaCl (11.5–19 wt% eq. NaCl approximately), the mode being around 5 mol% (Fig. 10 and Table 3).

Lw inclusions are aqueous inclusions with no detectable CO_2 and rather low (0.2 ± 0.1 mol% NaCl corresponding to approximately 0.5–0.9 wt% eq. NaCl) or high salinities around 8 mol% NaCl (range of 14–17 wt% NaCl). They occur in later FIP which have not been considered in this study.

5. Discussion

5.1. FI entrapment

Isochores were calculated for Lc-w inclusions using the equation of state from Bowers and Helgeson (1983) revised by Bakker (1999) for the H_2O–CO_2–CH_4–N_2–NaCl system. Isochores are reported as inset in Fig. 11 and used to provide information about the *P–T* conditions of vein formation. Errors on pressures linked to flw estimates (±5%) and approximation in V–X properties of fluids are estimated to be lower than ±150 bars at pressures higher than 2 kbar. As predictable, isochores of both primary and secondary Lc-w inclusions overlap in *P–T* space where they define a relatively broad band. Based on the calculated

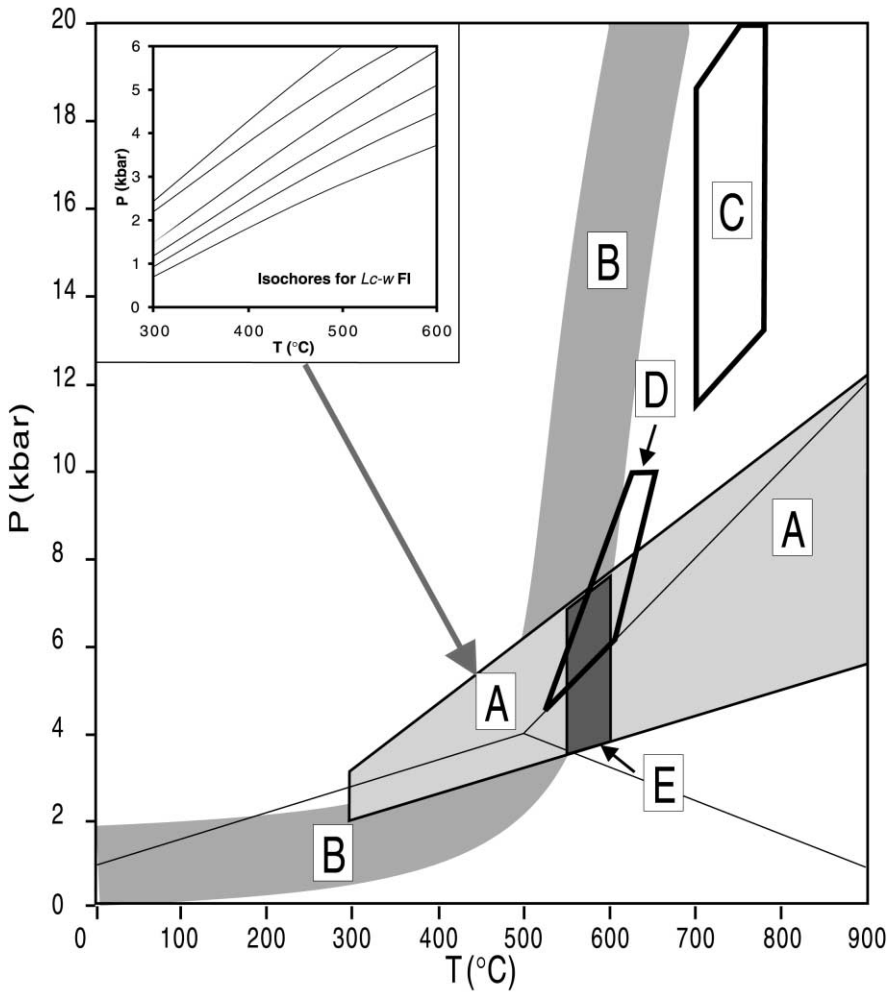

Fig. 11. *P–T* diagram constraining the possible trapping conditions of Lc-w FI: (A) field defined by isochores of primary and secondary Lc-w inclusions (see inset), (B) *P–T* path of Alpine metamorphism in the Tauern Window (Selverstone et al., 1984), (C) *P–T* conditions of Early Alpine metamorphism, (D) *P–T* conditions of Late Alpine metamorphism in adjacent metabasites (Barzi, 1996), (E) trapping conditions assuming a temperature range of 550–600°C (Hoernes and Friedrichsen, 1974).

isochores, conditions of fluid inclusion entrapment may be estimated using independent *P* or *T* constraints.

Geothermometric information on the Zentralgneis complex of the SW Tauern Window are scarce: the only data are the *T* estimates between 550 and 600°C of Hoernes and Friedrichsen (1974) and the *P–T* values of 530–650°C and >4.5 kbar of Barzi (1996). Additional constraints on temperature can be found in the mineral assemblage of host gneisses (Qtz–Oligoclase–Bt–Ms–Ep–Grt ± Kfs) which is considered by Le Goff (1989) as characteristic of $T \geq 560$°C. These data and the calculated isochores are represented in the *P–T* diagram in Fig. 11; also included is the *P–T–t* path of Selverstone et al. (1984) integrated by the radiometric data of Blanckenburg et al. (1989) which refers to the Upper and Lower Schieferhülle Units a few km to the west of the study area, and might not be coincident with that of the Zentralgneis complex. Under the assumptions that:

(1) the veins and the host rocks formed at the same *P–T* conditions during the thermal peak of the Tauern

metamorphism (Friedrichsen and Morteani, 1979); and

(2) the peak temperatures attained in the Neves area were between 550 and 600°C (Hoernes and Friedrichsen, 1974),

it follows that the pressures during vein formation and entrapment of primary Lc-w FI are between 3.5 and 7.5 kbar (box 'E' in Fig. 11). These estimates are in agreement with the data of both Selverstone et al. (1984) and Barzi (1996); they are slightly higher than pressures reported by Luckscheiter and Morteani (1980) which are generally <5 kbar. This discrepancy may be related to a different equation of state (not specified) used by Luckscheiter and Morteani (1980) for V–X calculations. Note that because the isochores for primary and secondary inclusions displaying the highest densities overlap in P–T space and intersect the possible Alpine P–T–t path at a single zone corresponding to the thermal peak of the Tauern metamorphism, the entrapment of secondary FI is likely to have occurred at the same conditions as the primary ones, i.e. after a very short time span.

The 3.5–7.5 kbar range of trapping pressures is certainly too large to represent a primary feature. The highest estimates can be interpreted as lithostatic or supra-lithostatic pressures in relation with the hydrofracturing mechanism at the origin of the vein system. They can also be considered as overestimates as they are calculated for the highest temperature range. If temperature decreased, especially during the trapping of the secondary inclusions, then corresponding pressures could be much lower (around 1–1.5 kbar less for a temperature drop of 100°C). Lower pressures may reflect (i) post-trapping changes, such as incipient decrepitation or loss of H_2O affecting the inclusions during the decompression path and/or (ii) pressure drops connected with the opening of the veins. The latter are of great importance for the process of quartz precipitation (see Section 5.2).

5.2. Metamorphic reactions in the host gneiss: origin of H_2O, CO_2 and chlorine

Origin of H_2O: In the perspective of modelling the veining events, it is relevant to constrain the possible metamorphic reactions occurring in the host rocks. In the Zentralgneis Complex, the almost isothermal decompression that took place between the high pressure Eo-Alpine metamorphism and the Tauern metamorphism event was accompanied by a pervasive post-tectonic recrystallization (Morteani, 1974). The most apparent result of this recrystallization is the reverse zoning of plagioclase which was explained by Hörmann and Raith (1973) as the result of reactions involving the simultaneous consumption of epidote muscovite and quartz and growth of biotite and/or K-feldspar. A similar reaction;

$$\mathrm{Ms + Grt + Ep + Pl_{core} + Qtz = Pl_{rim} + Bt + H_2O} \quad (1)$$

has been obtained by mass-balance calculations in one Kf-free host gneiss (Poletti 1997) using phase compositions as reported in Table 1. These are dehydration reactions, and their progress can be induced during near-isothermal decompression.

It follows that the H_2O component was released by the host gneisses during the Tauern metamorphism. A local derivation of the fluid is also suggested by the isotopic data of Hoernes and Friedrichsen (1974) on minerals from veins and host rocks indicating that water/rock ratio was probably low and the system closed.

Origin of CO_2: The CO_2 component, not considered in the reactions above, can be internally derived by decarbonation of the calcite present in the gneisses. In fact, calcite is an almost ubiquitous phase in the granitic gneisses of the area where it may be up to 5 vol% (Morteani and Raase, 1974). As most decarbonation equilibria have a positive slope in P–T space, we suggest that calcite in the host gneiss may also be involved as a reactant by a model reaction of the form:

$$\mathrm{Ms + Grt + Ep + Pl_{core} + Qtz + Cal = Pl_{rim} + Bt + H_2O + CO_2} \quad (2)$$

A devolatilization of this type could account for: (1) the observed zoning pattern of plagioclase, (2) the evidence of epidote replacement by biotite, and (3) the generation of a buffered H_2O–CO_2 mixture as determined in the FI of the veins.

Conversely, Luckscheiter and Morteani (1980) concluded that calcite was not abundant enough in the gneisses, and that the source of CO_2 was external to the vein–host rock system, to be found in the carbonate-rich rocks of the Schieferhülle. This was

considered as an evidence for long migration distances of decarbonation-released fluids as in many other examples in the Alps (e.g. Mullis et al., 1994).

However, studies of alpine clefts (e.g. Aar or Mont Blanc; Mullis et al., 1994; Cathelineau et al., 1995) show that CO_2 contents are rather variable when aqueous fluids are contaminated during the late stages by a CO_2-rich fluid percolating the main fault zones. This is difficult to reconcile with the evidence for restricted H_2O/CO_2 variations found in Lc-w FI that are more likely to be the result of a mixed dehydration–decarbonation reaction.

Origin of chlorine: The source of the rather high chlorine contents of FI is debatable as there are poor constraints on it. Chlorine can be internally derived by reactions involving Cl-bearing minerals, or introduced from an external source such as sedimentary or salt rich formations (Savoye et al., 1998).

An external source of high salinity fluids has been frequently proposed since prograde reaction are unlikely to produce significant amounts of Cl, contrary to retrograde reactions, namely chloritization of Cl-bearers such as amphibole or biotite. In this perspective, variations in chlorinity may indicate mixing between a high salinity component and a more dilute end-member.

On the other hand, the chemical composition of biotites indicates that Cl was available and in same amounts during (re)-crystallization of biotite in both veins and host rocks. Although this does not preclude the possibility of metasomatic processes by small scale infiltration of externally derived, saline fluids, this feature can be easily explained by the synchronous crystallization of biotite in both host rock and vein in the presence of a similar Cl-bearing fluid. The H_2O/Cl content of biotite (0.01–0.02) is about one-third of that in FI: this lower value is in agreement with the strong partitioning of Cl in fluids coexisting with biotite (Zhu and Sverjenski, 1991; Markl and Piazolo, 1998).

Regardless of the internal or external source of chlorine, starting from a fluid with moderate Cl content, higher and variable chlorinities can be subsequently obtained in the FI by a 'desiccation' process (e.g. Markl et al., 1998; Kullerud, 2000) of selective removal of H_2O in the crystallizing biotite. Partitioning of Cl between mineral and $H_2O–CO_2–NaCl$ fluids during decarbonation processes may eventually bring to the saturation of fluids with respect to salts (Trommsdorff et al., 1985).

5.3. A model for vein formation

Along with $P–T–X$ data from from FI, constraints to the model of Qtz–Pl–Bt vein formation come from the mineralogy of veins, that reflects the mineral assemblage of host gneisses. In particular, biotite and plagioclase in the vein have the same chemical composition as biotite and plagioclase rims in the host, which have been interpreted as the product assemblage of a metamorphic reaction occurring at the peak of the Tauern metamorphism.

As the proposed reaction (2) releases H_2O (and probably CO_2), it is able to determine the favourable conditions (pore fluid overpressure) for hydrofracturing of the host rocks. Vein opening by shear fracturing is less likely to have occurred as the extensive recrystallization accompanying metamorphism took place under static conditions.

Thus, in addition to the very rare occurrence of metasomatic halos around veins, a number of indications is in favour of a synmetamorphic veining event as modelled by Cesare (1994): rock hydrofracturing is induced by devolatilization reactions in the host and subsequent fluid migration and vein filling are internally controlled by the product phases and type of fluid released in the reaction. The result is a vein with a mineralogical and FI composition reflecting the product assemblage and $P–T$ conditions of devolatilizations in the adjacent host rock. Although originally proposed for a contact metamorphic regime, the synmetamorphic veining model can be applied (Cesare and Connolly, 1996) also to the low strain domains of regionally metamorphosed terrains, where low fluid infiltration and fluid–rock interaction are expected (Fig. 12). The Neves area, where the veins are found, fulfils this requisite as it is mainly composed by massive or weakly foliated gneisses of the Zentralgneis Complex grading to the south to a large belt of highly deformed rocks of the Lower and Upper Schieferhülle.

Concerning the Qtz–Pl–Bt veins, the synmetamorphic genetic model cannot account for the behaviour of quartz because reactions (1) and (2) proposed above are Qtz-consuming.

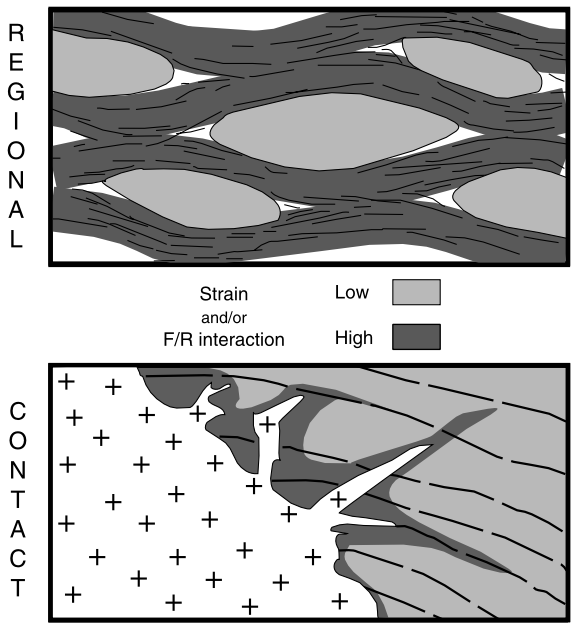

Fig. 12. Schematic representation of the distribution of high and low fluid–rock interaction areas in the regional (top) and contact (bottom) metamorphic scenarios. Synmetamorphic veining is likely to occur during metamorphism and devolatilization in the low strain and low fluid–rock interaction domains.

As quartz deposition occurred in veins after crystallization of biotite and plagioclase, we infer that a subsequent mechanism was active for the transfer of silica to the veins, and that it is reflected in the large P variations recorded by FI. These variations (a few kbar) reflect probably fluctuations below the lithostatic pressure in response to extensional opening of the fractures, and can account for significant changes in silica solubility leading to quartz precipitation in veins (Walther and Helgeson, 1977). Owing to the high solubility of silica in high temperature and pressure, dilute chloride fluids, effective mass transport occurs along pressure gradients from the host rocks (not necessarily adjacent to the fractures) to the forming extensional veins, and quartz is precipitated during P drops following microfracturing events. As this mechanism alone would require very large fluid/rock ratios, the efficiency of silica migration may have been increased by a concomitant mechanism of fluid pumping and reusing (Yardley and Bottrell, 1992).

6. Conclusions

Fluids found as primary and secondary Lc-w inclusions in veins from the highest temperature zone of the Zentralgneis Complex display similar composition and density and are likely to have been trapped at similar P–T values of 550–600°C and 3.5–7.5 kbar corresponding to the peak conditions of the Tauern metamorphism.

Although infiltration of externally derived fluids cannot be ruled out, the salinity and low carbonic content of Lc-w FI is compatible with a local derivation from the dehydrating/decarbonating host gneisses: this is consistent with the petrographic and chemical data (Morteani and Raase, 1974; this work) indicating that during the thermal peak of the Tauern metamorphism the gneisses were involved in devolatilization reactions such as

$$\mathrm{Ms + Ep + Grt + Pl_{core} + Qtz(+Cal)} = \mathrm{Pl_{rim} + Bt + H_2O(+CO_2)}$$

We propose that vein formation was triggered by such metamorphic devolatilization according to an initial synmetamorphic veining event with growth of biotite and plagioclase at vein walls.

The subsequent segregation of quartz towards vein centres is modelled by a process of silica transport and quartz precipitation mainly controlled by pressure fluctuations in the veins, possibly enhanced by fluid pumping and reusing (Yardley and Bottrell, 1992). Quartz occurrence might represent the evidence for the infiltration of externally derived fluids during veining, but the isotopic data of Hoernes and Friedrichsen (1974) indicate a complete equilibrium between vein and host quartz and would rather suggest either an internal fluid derivation or a deep equilibration with rocks.

The fluid chemistry is rather uncommon and characterized by significant changes in salinity from one FIP to the other. This indicates that a wide range of salinity in the fluid, all rather high, are linked to a process increasing Cl content (e.g. water removal or phase immiscibility) or to addition of Cl from an external source, not necessarily far from the studied area.

The synmetamorphic veining mechanism may be applicable only to the Qtz–Pl–Bt veins of the granitic

gneisses of the Neves area. Other veins and segregations consisting only of quartz, and occurring also in amphibolites, phyllites and calcschists in the western Tauern Window obviously require an alternative genetic model in which the source of silica is to be found outside the vein/host-rock system.

Acknowledgements

We wish to thank R. Bakker, J.L. Vigneresse and an anonymous reviewer for their careful reviews, M. Martini and G. Malghese for field assistance, C. Maineri for preliminary Raman analyses and L. Tauro for sample preparation. Financial supports come from MURST and CNR.

References

Bakker, R.J., 1997. Clathrates: Computer programs to calculate fluid inclusion V–X properties using clathrate melting temperatures. Comp. Geosci. 23, 1–18.

Bakker, R.J., 1999. Adaptation of the Bowers and Helgeson (1983) equation of state to the H_2O–CO_2–CH_4–N_2–NaCl system. Chem. Geol. 154, 225–236.

Barzi, L., 1996. Studio petrografico dei cumulati basici ed ultrabasici a sud-est della Cima di Campo — Turnerkamp (Alti Tauri–Alto Adige). Ump. Dipl. Thesis. University of Padova.

Barzi, L., Cesare, B., 1996. First occurrence of ultramafic cumulates in the Zentralgneis complex of the Tauern Window. Plinius 16, 31–32.

Blanckenburg, F.V., Villa, I.M., Baur, H., Morteani, G., Steiger, R.H., 1989. Time calibration of a PT-path from the Western Tauern Window, Eastern Alps: the problem of closure temperatures. Contrib. Mineral. Petrol. 101, 1–11.

Bowers, T.S., Helgeson, H.C., 1983. Calculation of the thermodynamic and geochemical consequences of non-ideal mixing in the system H_2O–CO_2–NaCl on phase relations in geologic system: metamorphic equilibria at high pressures and temperatures. Am. Mineral. 68, 1059–1075.

Cathelineau, M., Ayt Ougougdal, M., Banks, D., Lespinasse, M., Boiron, M.C., Poty, B., 1995. Fluids inputs and mass transfer during alpine brittle deformation of the Mont-Blanc. ECROFI XIII. Boll. Soc. Esp. Mineral. 18-1, 34–35.

Cesare, B., 1994. Synmetamorphic veining: origin of andalusite-bearing veins in the Vedrette di Ries contact aureole, Eastern Alps, Italy. J. Metamorph. Geol. 12, 643–653.

Cesare, B., Connolly, J.A.D., 1996. Devolatilization-generated veins in the lower crust: the synmetamorphic veining model. Goldschmidt Conference 1996, Heidelberg, Germany. J. Conf. Abstr. 1, 99.

Christensen, J.N., Selverstone, J., Rosenfeld, J.L., DePaolo, D.J., 1994. Correlation by Rb–Sr geochronology of garnet growth histories from different structural levels within the Tauern Window, Eastern Alps. Contrib. Mineral. Petrol. 118, 1–12.

D'Amico, C., 1974. Hercynian plutonism in the Alps. A report 1973–74 (Relazione ufficiale). Mem. Soc. Geol. It. 13, 49–118.

De Vecchi, G.P., Baggio, P., 1982. The Pennine Zone of the Vizze region in the western Tauern Window (Italian eastern Alps). Boll. Soc. Geol. It. 101, 89–116.

De Vecchi, G.P., Mezzacasa, G., 1986. The Pennine Basement and cover units in the Mesule group (South-western Tauern Window). Mem. Sci. Geol. 38, 365–392.

Dubessy, J., Larghi, L., Canals, M., 1997. Reconstitution of ionic composition of fluid inclusions. Proc. XIV ECROFI meeting, Boiron and Pironon, Nancy, pp. 90–91.

Finger, F., Frasl, G., Haunschmid, B., Lettner, H., von Quadt, A., Schermaier, A., Schindlmayr, A.O., Steyrer, H.P., 1993. The Zentralgneise of the Tauern Window (Eastern Alps): insight into an intra-Alpine Variscan Batolith. In: von Raumer, J.F., Neubauer, F. (Eds.), Pre-Mesozoic Geology in the Alps, pp. 375–391.

Friedrichsen, H., Morteani, G., 1979. Oxygen and hydrogen isotope studies on minerals from alpine fissures and their gneissic host rocks, Western Tauern Window (Austria). Contrib. Mineral. Petrol. 70, 149–152.

Frisch, W., Vavra, G., Winkler, M., 1993. Evolution of Penninic basement of the Eastern Alps. In: von Raumer, J.F., Neubauer, F. (Eds.), Pre-Mesozoic Geology in the Alps, pp. 349–360.

Hoernes, S., Friedrichsen, H., 1974. Oxygen isotope studies on metamorphic rocks of the western Hohe Tauern area (Austria). Schweiz. Min. Petr. Mitt. 54, 769–788.

Holland, T.J.B., 1979. High water activities in the generation of high pressure kyanite eclogites of the Tauern Window. Austr. J. Geol. 87, 127.

Hörmann, P.K., Morteani, G., 1972. Mineralogical and chemical composition of some carbonate minerals from the Zillerthal Alps, Tyrol (Austria). Tscherm. Miner. Petr. Mitt. 17, 46–59.

Hörmann, P.K., Raith, M., 1973. Bildungsbedingungen von Al–Fe(III)-Epidoten. Contrib. Mineral. Petrol. 38, 307–320.

Kerrick, D.M., 1990. The Al_2SiO_5 polymorphs. MSA Rev in Mineralogy, 22, 406 pp.

Kretz, R., 1983. Symbols for rock-forming minerals. Am. Mineral. 68, 277–279.

Kullerud, K., 2000. Occurrence and origin of Cl-rich amphibole and biotite in the Earth's crust — implications for fluid composition and evolution. In: Stober, Bucher (Eds.). Hydrogeology of Crystalline Rocks. Kluwer Academic Publishers, Holland, pp. 205–225.

Le Goff, E., 1989. Conditions pression-température de la déformation dans les orthogneiss: modèle thermodynamique et exemples naturels. Unp. PhD Thesis. University of Rennes.

Lhomme, T., Dubessy, J., Rull, F., 1999. Determination of chlorinity in aqueous fluids using Raman spectroscopy at room temperature. GeoRaman'99, Valladolid, Spain, pp. 93–94.

Luckscheiter, B., Morteani, G., 1980. Microthermometrical and chemical studies of fluid inclusions in minerals from Alpine veins from the penninic rocks of the central and western Tauern Window (Austria/Italy). Lithos 13, 61–77.

Markl, G., Piazolo, S., 1998. Halogen-bearing minerals in syenites

and high-grade marbles of Dronning Maud Land, Antartica: monitors of fluid compositional changes during late-magmatic fluid–rock interaction processes. Contrib. Mineral. Petrol. 132, 246–268.

Markl, G., Ferry, J., Bucher, K., 1998. Formation of saline brines and salt in the lower crust by hydration reactions and partially retrogressed granulites from the Lofoten Islands, Norway. Am. J. Sci. 298, 705–757.

Morteani, G., 1974. Petrology of the Tauern Window, Austrian Alps. Fortschr. Mineral. 52, 195–220.

Morteani, G., Raase, P., 1974. Metamorphic plagioclase crystallization and zones of equal anorthite content in epidote-bearing, amphibole-free rocks of the western Tauernfenster, eastern Alps. Lithos 7, 101–111.

Mullis, J., Dubessy, J., Poty, B., O'Neil, J., 1994. Fluid regimes during late stages of a continental collision: physical, chemical, and stable isotope measurements of fluid inclusions in fissure quartz from a geotraverse through the Central Alps, Switzerland. Geochim. Cosmochim. Acta 58, 2239–2267.

Oliver, N.H.S., 1996. Review and classification of structural controls on fluid flow during regional metamorphism. J. Metamorph. Geol. 14, 477–492.

Poletti, E., 1997. Vene Alpine negli Gneiss Centrali dei Tauri (Alpi Orientali): Studio delle inclusioni fluide. Unp. Dipl. Thesis. University of Padova.

Raith, M., 1971. Seriengliederung und Metamorphose im Östlichen Zillertaler Hauptkamm (Tirol/Österreich). Verh. Geol. B.A. 1, 163–207.

Raith, M., Raase, P., Kreuzer, H., Müller, P., 1978. The age of the Alpidic metamorphism in the Tauern Window, Austrian Alps, according to radiometric dating. In: Closs, H., Roedder, D., Schmidt, K. (Eds.), Alps, Apennines, Hellenides. Inter. Un. Comm. Geodyn. Sci. Rep. 38, 140–148.

Ramsay, J.G., 1980. The crack-seal mechanism of rock deformation. Nature 284, 135–139.

Roedder, E., 1984. Fluid inclusions. MSA, Rev. Mineral., 12, p. 646.

Sander, B., 1921. Geologische Studien am Westende der Hohen Tauern. Jb. Geol. St. A. Wien 70, 273–296.

Savoye, S., Aranyossy, J.F., Beaucaire, C., Cathelineau, M., Louvat, D., Michelot, J.L., 1998. Fluid inclusions in granites and their relationships with present day groundwater chemistry. Eur. J. Mineral. 10, 1215–1227.

Selverstone, J., 1985. Petrologic constraints on imbrication, metamorphism and uplift in the Tauern Window, eastern Alps. Tectonics 4, 687–704.

Selverstone, J., 1988. Evidence for east–west crustal extension in the Eastern Alps: implications for the unroofing history of the Tauern Window. Tectonics 7, 87–108.

Selverstone, J., Spear, F.S., Franz, G., Morteani, G., 1984. High pressure metamorphism in the S–W Tauern Window, Austria: *P–T* paths from horneblende–kyanite–staurolite schists. J. Petrol. 25, 501–531.

Trommsdorf, V., Skippen, G., Ulmer, P., 1985. Halite and sylvite as solid inclusions in high grade metamorphic rocks. Contrib. Mineral. Petrol. 89, 24–29.

Walther, R.K., Helgeson, H.C., 1977. Calculation of the thermodynamic properties of aqueous silica and the solubility of quartz and its polymorphs at high temperatures and pressures. Am. J. Sci. 277, 1315–1351.

Yardley, B.W.D., Bottrell, S.H., 1992. Silica mobility and fluid movement during metamorphism of the Connemara schist, Ireland. J. Metamorph. Geol. 10, 453–464.

Zhu, C., Sverjensky, D.A., 1991. Partitioning of F–Cl–OH between minerals and hydrothermal fluids. Geochim. Cosmochim. Acta 55, 1837–1858.